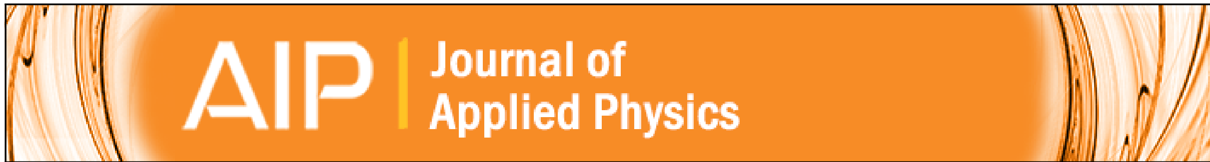

Physicochemical, structural, and mechanical properties of Si 3 N 4 films annealed in O 2

C. Aguzzoli, C. Marin, C. A. Figueroa, G. V. Soares, and I. J. R. Baumvol

Citation: Journal of Applied Physics **107**, 073521 (2010); doi: 10.1063/1.3359655
View online: http://dx.doi.org/10.1063/1.3359655
View Table of Contents: http://scitation.aip.org/content/aip/journal/jap/107/7?ver=pdfcov
Published by the AIP Publishing

Re-register for Table of Content Alerts

Create a profile.

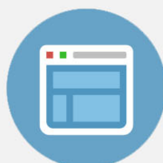

Sign up today!

[This article is copyrighted as indicated in the article. Reuse of AIP content is subject to the terms at: http://scitation.aip.org/termsconditions. Downloaded to] IP: 200.130.19.173 On: Fri, 21 Mar 2014 14:04:44

Physicochemical, structural, and mechanical properties of Si_3N_4 films annealed in O_2

C. Aguzzoli,[1,2] C. Marin,[1] C. A. Figueroa,[1] G. V. Soares,[1,a] and I. J. R. Baumvol[1,2]
[1]*Universidade de Caxias do Sul, Caxias do Sul, Rio Grande do Sul 95070-560, Brazil*
[2]*Instituto de Física, UFRGS, Porto Alegre, Rio Grande do Sul 91509-900, Brazil*

(Received 13 December 2009; accepted 6 February 2010; published online 14 April 2010)

The physicochemical, structural, and mechanical properties of silicon nitride films deposited by radio frequency reactive magnetron sputtering were investigated before and after thermal annealing in $^{18}O_2$. As-deposited films were essentially amorphous, stoichiometric, and free from contaminants for a wide range of deposition parameters, with hardness figures ranging from 16.5–22 GPa, depending mainly on the deposition temperature. After $^{18}O_2$ annealing at 1000 °C, films hardness converged to 21 GPa, independently of the deposition temperature, which is explained based on the crystallization of the films at this annealing temperature. Moreover, oxygen is incorporated only in 7.5 nm of the Si_3N_4, forming silicon oxynitride at the top surface of the film, indicating a good oxidation resistance at high temperature. Finally, the elastic strain to failure (H^3/E^2), which mimics the wear resistance of the film, doubles after the 1000 °C annealing. These observations show the great potential of silicon nitride as a hard coating for high temperature applications.
© *2010 American Institute of Physics*. [doi:10.1063/1.3359655]

I. INTRODUCTION

There is currently a crescent search for materials and surface coatings bearing high hardness and sufficient toughness at high temperatures. This is mostly concerned with tools for dry machining, cutting, and drilling, as well as dies for molten metal injection, and other applications.[1–3] Dry machining technology is ecologically and economically important, since the use, maintenance, and disposal of coolant lubricants entail enormous costs. Indeed, investigations show that in some cases the costs for using a coolant lubricant are many times higher than, for example, the tool costs.[4] Thus, coatings for cutting tools retaining combined hard and lubricating properties at high temperatures seem to be very interesting alternatives to reduce the enormous amounts of cooling emulsion and to work with minimal or no lubricant in a number of applications.[4,5] Moreover, energy generation related issues also demand coating for high temperatures applications, especially with high oxidation and corrosion resistance. For instance, to accomplish the next generation of coal power plants combustion engines in integrated gasification combined-cycle with 50% efficiency and zero emissions, they must operate at temperatures as high as 1400 °C.[6] In this way, the hot section of the turbine will require coatings to fulfill these new demands. New nuclear fission and fusion technologies will also require coatings with oxidation and corrosion resistance properties in extreme operation conditions.

The drawbacks of the well known Ti-based coatings have strongly limited their applications at high temperatures. This results in a challenge, since most high temperature coatings rely on the formation of a protective oxide scale by interaction with the environment. This scale must fulfill several requirements, like being stable, dense, and adherent, growing slowly, besides of bearing high temperature hardness, low friction coefficient, and wear and corrosion resistance. These conditions are in general not fulfilled by Ti-based coatings above 800 °C. However, in dry machining the cutting tool edge may reach well above 800 °C,[7] a temperature at which most of the Ti-based coatings degrade due to oxidation, corrosion, and formation of a porous, nonprotective oxide scale. New coatings are being developed for high temperature applications, such as AlCrN, WC/C, as well as several multilayered coatings.[1–3,8,9]

Silicon nitride is a promising coating candidate for high temperature tools, die coatings, and other engineering components owing to its reasonably high hardness, combined with thermodynamical stability, corrosion resistance, and oxidation resistance at the high temperatures addressed.[10–13] Since most of the hard coatings investigated so far loose substantially their hardness when submitted to high temperatures, either at work or in laboratory furnace heating, it is very useful to know whether the hardness and elastic modulus of silicon nitride coatings would be retained up to temperatures of practical interest, such as 1000 °C. Another aspect of major interest for practical purposes would be the thickness, composition, and adherence of any eventual oxide or oxynitride layer formed due to high temperature processing that can act as a protective and lubricant layer near the silicon nitride film surface. Previous studies of silicon oxynitride films showed that hardness and Young modulus increased with increasing nitrogen content[14] from SiO_2 to Si_3N_4. Furthermore, the existence of Si–N bonds embedded in Si–O matrix tended to enhance these magnitudes, approaching the values of silicon nitride.[15,16]

Many deposition techniques have been used to deposit Si_3N_4 films, such as chemical vapor deposition (CVD), plasma enhanced CVD, and magnetron sputtering.[17] Among them, deposition by magnetron sputtering can lead to several

[a]Electronic mail: gvsoares@gmail.com.

 © 2010 American Institute of Physics

[This article is copyrighted as indicated in the article. Reuse of AIP content is subject to the terms at: http://scitation.aip.org/termsconditions. Downloaded to] IP: 200.130.19.173 On: Fri, 21 Mar 2014 14:04:44

TABLE I. Deposition parameters for Si_3N_4 films.

Base pressure (mbar)	5×10^{-7}
Ar partial pressure (mbar)	3×10^{-3}
N_2 partial pressure (mbar)	$0.7-12\times10^{-3}$
RF power density (W cm^{-2})	7.7
Substrate temperature (°C)	23–500
Deposition time (s)	15–3000
Target to substrate distance (mm)	60

advantages, such as: (a) low substrate temperature during deposition, since in the CVD process deposition temperatures can be as high as 800 °C, (b) wide acceptance by the industrial sector, making it easy to scale up the process, (c) elimination of hydrogen in the films, since hydrogenated silicon nitride films present inferior thermal stability,[18] and (d) elimination of toxic gases in the deposition process, such as NH_3 and SiH_4.

Mechanical properties of Si_3N_4 thin films at high temperature have not been found in the literature by the present authors. However, thermal stability has been addressed,[11] showing that even for temperatures far above 1000 °C and rather long annealing times, the amorphous as-deposited films are transformed in a mixture of the stable β-Si_3N_4 and the metastable α-Si_3N_4 phases.

Finally, the hardness to Young modulus (H/E) ratio, so called elastic strain to failure, has been proposed and consistently used to evaluate the resistance to plastic deformation of thin film coatings.[19–22] More specifically, the H^3/E^2 ratio is considered to be a good indicator of the coating resistance to wear. Thus, a high H^3/E^2 indicates a high resistance of the coating to plastic deformation and, presumably, a high wear resistance as well, besides of low stiffness.[23,24] Therefore, the temperature dependence of H^3/E^2 is also determined here for the Si_3N_4 films.

In the present work we investigated the physicochemical, mechanical, and structural properties of the Si_3N_4 films deposited on Si by radio frequency (rf) reactive magnetron sputtering, before and after annealing in oxygen.

II. EXPERIMENTAL

Silicon nitride (Si_3N_4) films were deposited on Si(001) and on amorphous carbon substrates by rf reactive magnetron sputtering. Prior to deposition, substrates were cleaned by ultrasonic acetone bath and immediately loaded in the sputtering vacuum chamber, which was pumped down to a base pressure of 5×10^{-7} mbar. Silicon substrates were submitted to an additional cleaning step in 10% hydrofluoridric acid solution, after the ultrasonic acetone bath. A 2 in. high purity (>99.99%) silicon target was used, located 60 mm away from the substrate of interest, and Si_3N_4 film depositions were performed using a mixture of argon and nitrogen gases, with a constant argon partial pressure of 3×10^{-3} mbar and a variable N_2 partial pressure. An input rf power density of 7.7 W cm^{-2} was employed with a reflected power density lower than 0.05 W cm^{-2}. The substrate temperature was varied from room temperature (23 °C) to 500 °C. No substrate bias was applied and no delamination of the films was observed in all cases. Table I summarizes the deposition parameters.

In order to investigate the thermal stability and oxidation resistance of the as-deposited Si_3N_4 coatings, samples were loaded in a static pressure resistively heated quartz furnace, which was pumped down to 2×10^{-7} mbar, before being pressurized with oxygen enriched to 97% in the isotope of mass 18, hereafter called $^{18}O_2$ annealing. Annealing was performed in 100 mbar of $^{18}O_2$ for 1 h, at three different temperatures, namely, 250, 500, and 1000 °C. The use of the ^{18}O rare isotope allows us to distinguish it from oxygen previous incorporated in the films due to contamination or due to atmospheric air exposure.

The elementary composition of the films was evaluated by Rutherford backscattering spectrometry (RBS) using a 2 MeV He^+ beam and a backscattering detection angle of 165°, bearing a sensitivity of 10^{14} atm cm^{-2} (about 1/10 of a monolayer) and 10% accuracy.[25] The crystalline structure of the films was determined by grazing incidence angle x-ray diffraction (GAXRD) using a constant incident angle of 1° and Cu K_α radiation ($\lambda=1.5418$ Å). Film densities were obtained from x-ray reflectometry (XRR) measurements using Cu K_α radiation and scanning in 0.002° steps. XRR data were simulated using the Parratt formalism for reflectivity.[26] The hardness and reduced elastic modulus were accessed by the nanoindentation technique with a Berkovich indenter, a load rate of 0.03 mN s^{-1} and a maximum indentation depth of 20 nm. ^{18}O and ^{15}N profiles were determined by narrow nuclear resonant reaction profiling[27] (NRP) using the narrow resonances ($\Gamma=100$ and 120 eV) in the cross section curves of the $^{18}O(p,\alpha)^{15}N$ and $^{15}N(p,\alpha\gamma)^{12}C$ nuclear reactions at 151 keV and 429 keV, respectively. Simulations of the nuclear reaction excitation curves were carried out using the FLATUS code.[28] Although ^{14}N is the most abundant nitrogen isotope (99.6%), the NRP technique is sensitive enough to profile the ^{15}N isotope present in the Si_3N_4 films, with a natural abundance of 0.4%. X-ray photoelectron spectroscopy (XPS) was performed using Mg K_α radiation (1253.6 eV) at a take-off angle of 60° in order to evaluate the Si and N chemical environments.

III. COMPOSITION, STRUCTURE, AND MECHANICAL PROPERTIES OF THE AS-DEPOSITED Si_3N_4 FILMS

Figure 1(a) shows a typical RBS spectrum of a Si_3N_4 film, in this case deposited on carbon, at a substrate temperature of 200 °C for 300 s (solid circles). Carbon is used as substrate in the RBS measurements in order to eliminate the high background signal from the more commonly used Si substrate. In this figure one can see the N and Si signals from the silicon nitride film, as well as some Ar incorporated during the sputtering process. The element areal densities are proportional to the areas under the corresponding peaks. This spectrum also shows that the films are free from contaminants such as O and Fe, within the RBS sensitivity, which could modify several of their properties, such as hardness and adhesion.[29,30] In Fig. 1(b), the Si to N ratio is presented as a function of N_2 partial pressure during deposition for two

[This article is copyrighted as indicated in the article. Reuse of AIP content is subject to the terms at: http://scitation.aip.org/termsconditions. Downloaded to] IP: 200.130.19.173 On: Fri, 21 Mar 2014 14:04:44

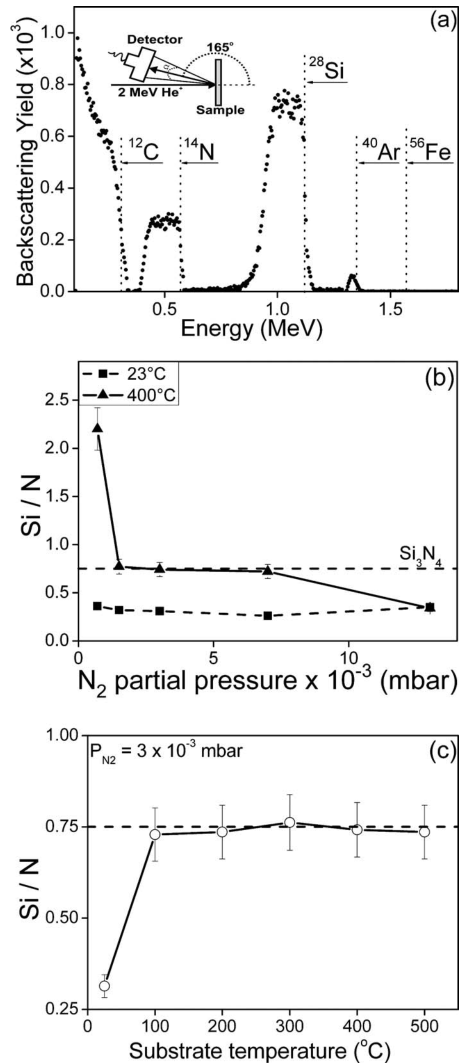

FIG. 1. (a) Rutherford backscattering spectroscopy spectrum from a Si_3N_4 film deposited on carbon at 200 °C (solid circles). The different elements present in the sample are indicated as well as the position for the Iron (^{56}Fe) signal. Inset: experimental setup for the RBS analyses. (b) Silicon to nitrogen ratio in Si_3N_4 films deposited at 400 °C (solid triangles and solid line) and room temperature (solid squares and dot line) as a function of the N_2 partial pressure during deposition. The dashed line represents the optimal Si/N ratio. (c) Silicon to nitrogen ratio for Si_3N_4 films (open circles) deposited with a N_2 partial pressure of 3×10^{-3} mbar as a function of the deposition temperature. Lines are only to guide the eyes.

substrate temperatures, room temperature (solid squares and dashed line) and 400 °C (solid triangles and solid line), while keeping a constant Ar partial pressure of 3×10^{-3} mbar. The total pressure during deposition can be calculated adding the Ar partial pressure to the N_2 partial pressure. The straight dashed line shows the Si to N atomic ratio for stoichiometric Si_3N_4, namely 0.75. For depositions at room temperature, no stoichiometric silicon nitride is observed for any N_2 partial pressure used, indicating an N excess in the films. At 400 °C, we observe a Si excess for depositions at N_2 partial pressures below 1×10^{-3} mbar, while an N excess is observed for N_2 partial pressure above 7×10^{-3} mbar. Between 1 and 7×10^{-3} mbar, stoichiometric silicon nitride is formed at 400 °C. Further depositions were carried out using a N_2 partial pressure of 3×10^{-3} mbar, in order to keep the total pressure during deposition (6×10^{-3} mbar in this case) as low as possible, maximizing the mean free path in the deposition chamber. Using this Ar and N_2 constant partial pressures, we investigated the stoichiometry of the films as a function of the substrate temperature during deposition, showed in Fig. 1(c). We observed that only for room temperature deposition, the silicon nitride film is not stoichiometric, while for all other temperatures used, Si_3N_4 is observed. This result indicates that some activation energy, higher than the energy provided at room temperature, is necessary to obtain stoichiometric silicon nitride. It is important to remember that several properties of silicon nitride depend on stoichiometry, such as refraction index and hardness.[14,31] Moreover, the possibility to obtain Si_3N_4 films at substrate temperatures as low as 100 °C, allows the deposition of silicon nitride in different kinds of substrates.

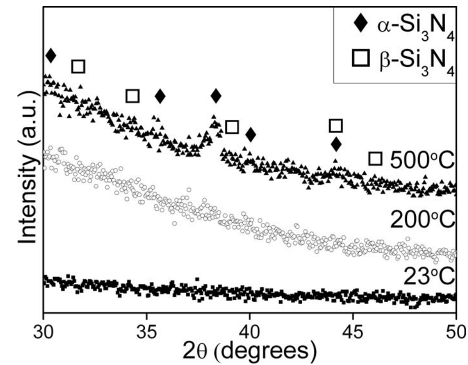

FIG. 2. Grazing angle x-ray diffraction of Si_3N_4 films deposited at 23 °C (solid squares), 200 °C (open circles), and 500 °C (solid triangles). The positions of the main diffraction peaks from α-Si_3N_4 (solid lozenge) and β-Si_3N_4 (open squares) are indicated. (a.u.=arbitrary units).

GAXRD results are shown in Fig. 2 for Si_3N_4 films deposited on Si at substrate temperatures of 23 °C (solid squares), 200 °C (open circles), and 500 °C (solid triangles). The positions of the main diffraction peaks of the α-Si_3N_4 (open squares) and β-Si_3N_4 (solid lozenges) phases are also indicated. It can be seen that the films are essentially amorphous after deposition, except for the deposition at 500 °C where some diffraction peaks attributed to the α-Si_3N_4 phase are observed, which is considered a metastable phase. We must stress that the crystalline structure of the coatings plays an important role in mechanical properties, since the crystalline phases of silicon nitride are harder than the amorphous phase.[32,33] This point will be discussed below, following the annealing results.

In order to convert the N areal densities obtained from RBS to film thickness, it is important to determine the density of the films. Moreover, a correlation between the mechanical properties of silicon nitride films and its density has been proposed.[34] In this way, the Si_3N_4 density was determined using the XRR technique, from which it is also possible to evaluate the abruptness of the interface between the film and the substrate. Figure 3 shows the XRR data from a Si_3N_4 film deposited at 200 °C for 30 s (solid squares) and the simulation (line). The results from the simulation are shown in the inset, where a density of 3.01 g cm^{-3} and a thickness of 55 nm were obtained. The density figure is in good agreement with previous results[34,35] for amorphous

[This article is copyrighted as indicated in the article. Reuse of AIP content is subject to the terms at: http://scitation.aip.org/termsconditions. Downloaded to] IP: 200.130.19.173 On: Fri, 21 Mar 2014 14:04:44

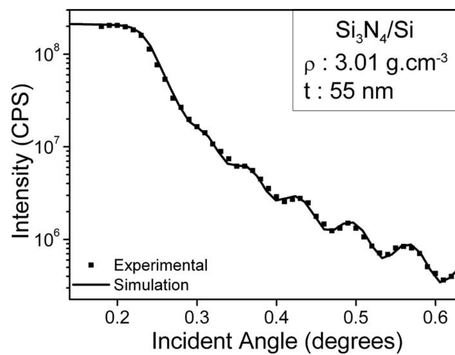

FIG. 3. XRR data (solid squares) of Si_3N_4 films deposited on Si at 200 °C for 30 s and the respective simulation (solid line). The density (in g cm^{-3}) and the thickness (in nanometer) of the film obtained from the simulation are presented in the inset. CPS stands for counts per second.

Si_3N_4 films. Considering the density from the XRR simulation, a relation between the total N amount and the film thickness was calculated,

$$10^{15}\ \text{N cm}^{-2} = 0.18\ \text{nm}. \tag{1}$$

The simulation also shows that the roughness of the interface between Si_3N_4 and Si is about 1 nm.

Figure 4(a) shows the N and Si areal densities in Si_3N_4 films deposited at 200 °C as a function of deposition time. The vertical scale is logarithmic for better visualization. The N and Si total amounts show a linear increase with deposition time, as well a 0.75 Si to N ratio for all deposition times employed. Using relation (1) we convert the total N amount to Si_3N_4 film thickness, showed in Fig. 4(b). A linear relation between film thickness and deposition time was obtained, with a deposition rate of 1.6 nm/s (~0.5 μm/h). This is a necessary relationship for any practical application, since the thickness of the coating plays an important role. In this way,

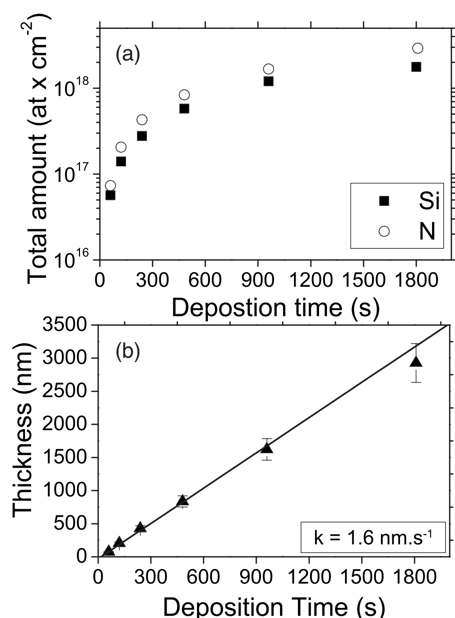

FIG. 4. (a) Silicon and nitrogen total amounts in Si_3N_4 films deposited at 200 °C as a function of deposition time. (b) Thickness of Si_3N_4 films as a function of deposition time. The deposition rate (k) obtained from linear fit of the data is presented.

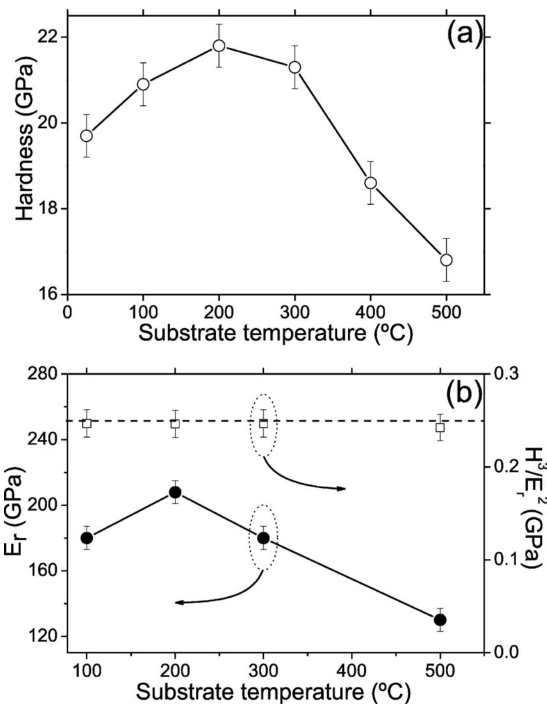

FIG. 5. (a) Hardness (open circles) of the Si_3N_4 films as a function of deposition temperature. (b) Left-hand side: reduced elastic modulus (solid circles) as a function of deposition temperature. Right-hand side: H^3/E_r^2 (open squares) as a function of deposition temperature. Lines are only to guide the eyes.

to determine the mechanical properties of the films, a deposition time of 120 s was used, yielding a film thickness of 192 nm. Since in the nanoindentation measurements a maximum depth of 20 nm was used, only 10% of the film thickness is probed, eliminating the substrate contribution.

Figure 5(a) shows the hardness (open circles) of the Si_3N_4 films deposited on Si as a function of substrate temperature during deposition. Each point is obtained from an average of 20 measurements in different spots on the sample surface. A small increase in hardness is observed when the substrate temperature is increased from 23 to 200 °C. This hardness figures (19.5–22 GPa) are consistent with those for amorphous silicon nitride reported in the literature.[14,34,36] However, when the substrate temperature is increased from 200 to 500 °C, a reduction in hardness is observed from 22 to 16.5 GPa. Before discussing the observed behavior of Si_3N_4 film hardness with temperature, we must make some considerations regarding the internal stress of the films. Previous results in metal nitride films deposited by sputtering, like AlN and MoN_x, show that the gas pressure during deposition determines the type of intrinsic residual stress in the films.[37,38] For deposition pressures below 13×10^{-3} mbar, the internal stress is essentially compressive, while above this pressure the stress becomes tensile. Since our depositions were performed at 6×10^{-3} mbar, we assume that the internal stress of the present films is compressive. Moreover, the origin of the residual stress can be attributed to the thermal residual stress (extrinsic) and to the intrinsic stress due to the film growth process. However, the coefficient of thermal expansion of the silicon substrate ($\sim3.5-4\times10^{-6}$/K) (Ref. 39) and that of Si_3N_4($\sim3-3.7\times10^{-6}$/K) (Ref. 40) are

[This article is copyrighted as indicated in the article. Reuse of AIP content is subject to the terms at: http://scitation.aip.org/termsconditions. Downloaded to] IP: 200.130.19.173 On: Fri, 21 Mar 2014 14:04:44

rather similar, making the residual thermal stress contribution negligible. In this way, the increase in hardness observed in the 23 and 200 °C substrate temperature range is attributed to an increase in the compressive internal stress of the film. Indeed, correlations between hardness increase and compressive internal stress increase, in some cases linear correlations, have been reported[41–43] for TiN, ZrN, and TiC_xN_{1-x} films deposited on different types of substrates, corroborating our assumption. The decrease in hardness observed for temperatures above 200 °C is attributed to the relaxation of the compressive internal stress, since the beginning of the crystallization of the Si_3N_4 film, observed for sample deposited at 500 °C, helps the relaxation of the internal stress, thus reducing the hardness. Although the internal stress of the films were not measured here, this behavior has been observed previously[44] in the deposition of SiC films on Si. Figure 5(b) shows the reduced elastic modulus (solid circles, left-hand side) obtained from the load-displacement curves and the elastic strain to failure H^3/E^2 (open squares, right-hand side). The reduced elastic modulus behavior is similar to the hardness behavior, a slight increase in the 23–200 °C substrate temperature range and a decrease in the 200–500 °C range. This can be explained with the same argument presented above of increase in the internal stress, and further relaxation for higher substrate temperatures. Correlation between the compressive internal stress and the elastic modulus has also been reported.[42] Although the modulations in the internal stress help to explain the observed variations in hardness, other mechanisms cannot be disregarded, such as grain size changes and point defects in the films. Moreover, the complicated interplay between the different factors affecting films hardness still remains as a point of discussion, especially in superlattice structures. The H^3/E^2, commonly used to foresee the wear resistance of coatings, remains constant (0.25 GPa) for all substrate temperature used in this work. This happens since the increase/decrease in hardness is followed by the same increase/decrease in the reduced elastic modulus when the substrate temperature is varied.

IV. MECHANICAL AND STRUCTURAL PROPERTIES OF SI_3N_4 FILMS AFTER $^{18}O_2$ ANNEALING

The hardness of Si_3N_4 films deposited at different substrate temperatures, namely 100 °C (solid squares and dashed line), 200 °C (open circles and solid line), and 500 °C (solid triangles and dotted line), as a function of annealing temperature in $^{18}O_2$ are shown in Fig. 6(a). In the three samples, a reduction in hardness is observed annealing at 250 °C, while for annealing at 500 °C, the sample deposited at 200 °C presents a progressive decrease in hardness, but samples deposited at 100 and 500 °C show some increase. This is once again attributed to changes in the internal stress of the films. Since the sample deposited at a substrate temperature of 200 °C presents the highest hardness after deposition, it should present the highest internal stress. Following this reasoning, the annealing at 250 and 500 °C induces a relaxation of this stress, reducing the hardness of the film. The pictures changes for the sample deposited at

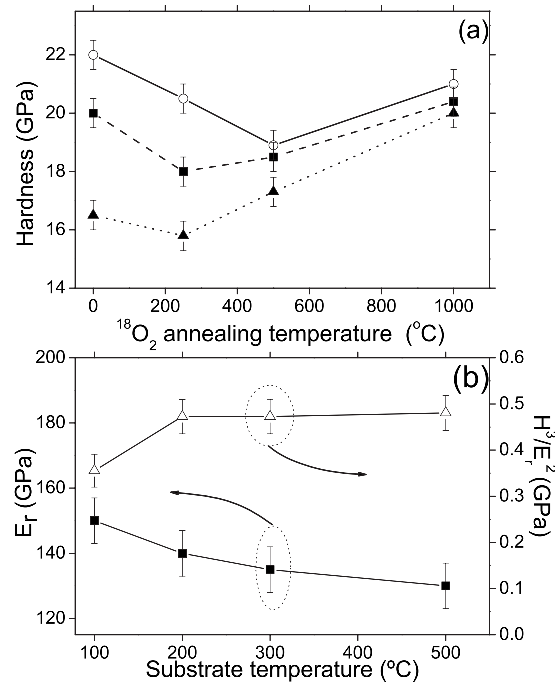

FIG. 6. Hardness of Si_3N_4 films deposited at 100 °C (solid squares), 200 °C (open circles), and 500 °C (solid triangles) as a function of $^{18}O_2$ annealing temperature. (b) Left-hand side: reduced elastic modulus (solid squares) as a function of deposition temperature after $^{18}O_2$ annealing at 1000 °C. Right-hand side: H^3/E_r^2 (open triangles) as a function of deposition temperature after $^{18}O_2$ annealing at 1000 °C. Lines are only to guide the eyes.

500 °C, since it has a lower hardness, it should also present a lower internal stress. In this way, the annealing at 250 °C may induce some relaxation of the remaining internal stress, but the effect is less pronounced than for the 200 °C sample. When the annealing is performed at 500 °C, an increase in hardness is observed, which should be related to a different process, rather than increase/decrease of the internal stress. The sample deposited at 100 °C presents a similar, although less pronounced, behavior as compared to the sample deposited at 500 °C. Finally, when the annealing is performed at 1000 °C, all investigated samples present an increase in hardness, approaching the same value (within the experimental error), namely 21 GPa. This effect will be discussed below in conjunction with the structural properties of the annealed films. Since the samples annealed at 1000 °C present an increase in hardness, which is a highly desirable effect for hard coatings in high temperature applications, we investigated other mechanical properties of the films deposited at different substrate temperatures after the 1000 °C annealing. Figure 6(b) shows the reduced elastic modulus (solid squares, left-hand side) obtained from the load-displacement curves and the elastic strain to failure H^3/E^2 (open triangles, right-hand side) for Si_3N_4 films after the 1000 °C annealing, as a function of substrate temperature during deposition. Here we used the reduced elastic modulus to estimate the elastic strain to failure (H^3/E^2). A progressive reduction in the reduced elastic modulus after 1000 °C annealing is observed when the substrate temperature is increased, except for the sample deposited at 500 °C. This sample presents the same E_r before and after annealing, as shown in Figs. 5(b)

[This article is copyrighted as indicated in the article. Reuse of AIP content is subject to the terms at: http://scitation.aip.org/termsconditions. Downloaded to] IP: 200.130.19.173 On: Fri, 21 Mar 2014 14:04:44

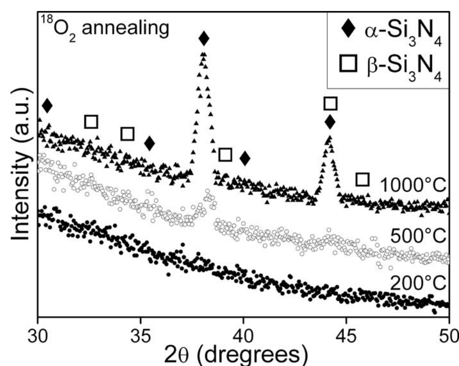

FIG. 7. Grazing angle x-ray diffraction of Si_3N_4 films deposited at 200 °C (solid circles) and after $^{18}O_2$ annealing at 500 °C (open circles) and 1000 °C (solid triangles). The positions of the main diffraction peaks from α-Si_3N_4 (solid lozenge) and β-Si_3N_4 (open squares) are indicated.

and 6(b). This indicates that the properties of the Si_3N_4 films after deposition (before annealing) play some role on the mechanical properties after annealing. Composition differences cannot account for this, since all films are stoichiometric and free from contaminants. However, their structures present some differences, as presented in Fig. 2 where the sample deposited at 500 °C has some crystalline order, while for all (not shown) other temperatures investigated, the films are amorphous. In this way, the decrease in the reduced elastic modulus for samples deposited at 100, 200, and 300 °C after annealing at 1000 °C, may be related to some structural changes in the films and/or to changes in the internal stress. The elastic strain to failure H^3/E^2 presented in the right-hand side of Fig. 6(b) also present some changes after the 1000 °C annealing. Here we observe a considerable increase in the H^3/E^2 for all samples after annealing from 0.25 to 0.4–0.48 GPa, which his close to a factor of 2. This is another highly desirable effect for high temperatures applications.

Figure 7 shows the GAXRD of Si_3N_4 films as-deposited at a substrate temperature of 200 °C (solid circles) and after $^{18}O_2$ annealing at 500 °C (open circles) and 1000 °C (solid triangles). According to Fig. 2, the as-deposited sample is essentially amorphous. However, annealing at 500 °C induces partial crystallization in the form of α-Si_3N_4. The crystallization becomes more pronounced when the annealing is performed at 1000 °C, although other diffraction peaks from the α-Si_3N_4 phase were not observed, possibly due to preferential orientation. Si_3N_4 crystallization induced by annealing has been reported,[11] where the authors showed that the β-Si_3N_4 phase is observed only at higher annealing temperatures and times, namely 1600 °C and 8 h, respectively. We attribute the increase in hardness and the decrease of the reduced elastic modulus after annealing at 1000 °C observed in Fig. 6(a) to this crystallization process, since the crystalline phase of Si_3N_4 is harder than the amorphous phase. Indeed, the behavior observed in Fig. 6(a) is attributed to a competitive process between internal stress relaxation (decreasing hardness) and crystallization (increasing hardness). In the sample deposited at 200 °C and annealed at 250 and 500 °C, internal stress relaxation is favored, since the annealing temperature is not high enough to induce significant

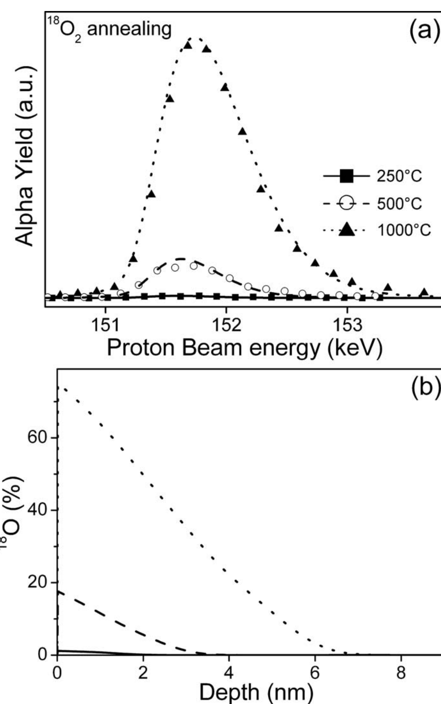

FIG. 8. Experimental excitation curves (symbols) of the $^{18}O(p,\alpha)^{15}N$ nuclear reaction around the resonance energy E_r=151 keV and the corresponding simulations (lines) for samples annealed in $^{18}O_2$ at 250 °C (solid squares and solid line), 500 °C (open circles and dashed line), and 1000 °C (solid triangles and dotted line). (b) ^{18}O profiles obtained from the simulation of the excitation curves presented in (a). Line types are the same as in (a). ^{18}O concentration is normalized to oxygen in stoichiometric SiO_2.

crystallization. When the annealing is performed at 1000 °C, the crystallization is favored and the hardness is increased. This competitive process also happens to a certain extent in samples deposited at 100 and 500 °C. Moreover, we cannot disregard that during the $^{18}O_2$ annealing, oxidation of the Si_3N_4 may take place, as well as the fact that silicon oxide (SiO_2) and silicon oxynitrides (SiO_yN_x) present lower hardness figures[14,36] than stoichiometric Si_3N_4, either in amorphous or crystalline forms. In this way, the formation of some oxide or oxynitride layer may contribute to a reduction in hardness, but this reduction can be compensated by the crystallization process. The next section will show results in oxygen and nitrogen atomic transport during annealing that shed some light into this issue.

V. OXYGEN AND NITROGEN ATOMIC TRANSPORT IN Si_3N_4 DURING $^{18}O_2$ ANNEALING

Figure 8(a) shows the experimental excitation curves (symbols) for the $^{18}O(p,\alpha)^{15}N$ nuclear reaction around the resonance energy E_r=151 keV and the corresponding simulations (lines) for Si_3N_4 deposited at 200 °C for 120 s and annealed in $^{18}O_2$ at 250 °C (solid squares and solid line), 500 °C (open circles and dashed line), and 1000 °C (solid triangles and dotted line). From the simulations is possible to obtain the ^{18}O profiles presented in Fig. 8(b), where the y-axis stand for ^{18}O concentration normalized for oxygen in stoichiometric SiO_2. Sample annealed at 250 °C (solid line) presents small ^{18}O incorporation, only 1.2% and 2 nm in depth. When the annealing temperature is increased to

[This article is copyrighted as indicated in the article. Reuse of AIP content is subject to the terms at: http://scitation.aip.org/termsconditions. Downloaded to] IP: 200.130.19.173 On: Fri, 21 Mar 2014 14:04:44

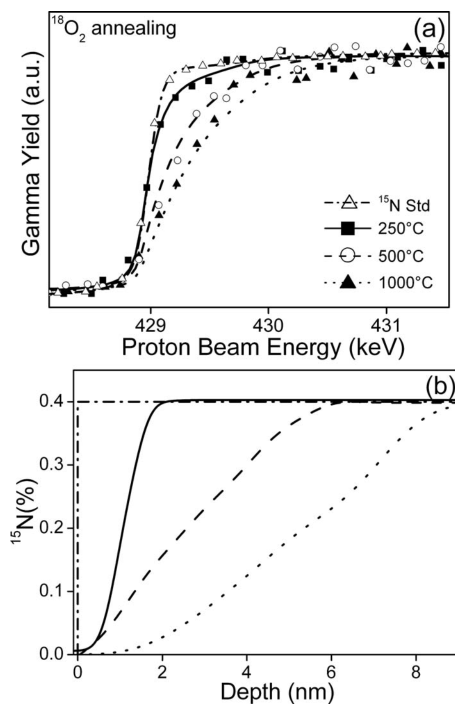

FIG. 9. Experimental excitation curves (symbols) of the $^{15}N(p,\alpha\gamma)^{12}C$ nuclear reaction around the resonance energy E_r=429 keV and the corresponding simulations (lines) for the as-deposited sample (open triangles and dashed-dotted line) as well as for samples annealed in $^{18}O_2$ at 250 °C (solid squares and solid line), 500 °C (open circles and dashed line), and 1000 °C (solid triangles and dotted line). (b) ^{15}N profiles obtained from the simulation of the excitation curves presented in (a). Line types are the same as in (a). ^{15}N concentration of 0.4% corresponds to stoichiometric Si_3N_4.

500 °C, ^{18}O incorporation increases to 18% close to the film surface, but again in a narrow region of the film surface, only 3.5 nm. Annealing at 1000 °C leads to 75% incorporation near the surface, but located only 7 nm away from the film top surface. Moreover, the shape of the profiles at 500 and 1000 °C annealing resembles a diffusion limited process, close to an complementary error function (ercf)-like profile. It must be pointed out that Si_3N_4 is commonly used as a diffusion barrier in the microelectronic industry. This results show the great oxidation resistance of the Si_3N_4 submitted to thermal annealing, since even after annealing at 1000 °C for a 1 h, oxygen is incorporated only in 7 nm in depth. The oxygen atoms incorporated therein may react with the Si_3N_4 network forming silicon oxynitride or silicon oxide. Indeed, tribological properties (friction and wear rate) of monolithic Si_3N_4 containing different crystalline phases were reported[45] showing that the friction coefficient and wear rate were reduced when surface layers, such as SiO_2, and SiO_xN_y, were formed during tribological tests at 1000 °C. However, when the tests were performed at 400 °C, no reduction in the wear rate and friction coefficient was observed, since at this temperature no significant layer of silicon oxynitride or silicon oxide is formed, as shown in this work.

Figure 9(a) shows the experimental excitation curves (symbols) for the $^{15}N(p,\alpha\gamma)^{12}C$ nuclear reaction around the resonance energy E_r=429 keV and the corresponding simulations (lines) for Si_3N_4 deposited at 200 °C for 120 s (open triangles and dashed-dotted line) and annealed in $^{18}O_2$ at 250 °C (solid squares and solid line), 500 °C (open circles

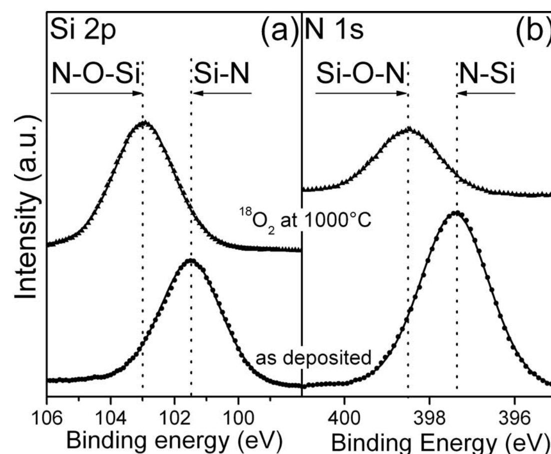

FIG. 10. (a) Si 2*p* and (b) N 1*s* x-ray photoelectron spectra (a.u. =arbitrary units) at take-off angle of 45° for Si_3N_4 films deposited at 200 °C (solid circles and solid line) and after $^{18}O_2$ annealing at 1000 °C (solid triangles and solid line). Energy positions for Si–N and Si–O–N environments are indicated. Lines stand for fittings.

and dashed line) and 1000 °C (solid triangles and dotted line). From the simulation it is possible to obtain the ^{15}N profiles presented in Fig. 9(b). The 0.4% ^{15}N concentration in *y*-axis of Fig. 9(b) stands for N concentration in stoichiometric silicon nitride, since this is the isotopic natural abundance of ^{15}N. Nitrogen profile of the as-deposited sample (open triangles and dashed-dotted line) is a horizontal straight line at 0.4% in N concentration, indicating the deposition of a homogeneous and stoichiometric silicon nitride. After annealing at 250 °C (solid square and solid line), we observe a small variation in N distribution, only 1 nm in depth from the film surface. However, when the sample is annealed at 500 °C, nitrogen is partially removed from the film in a 5 nm thick region, whereas annealing at 1000 °C removes nitrogen from an 8 nm thick region. Comparing the regions where nitrogen was removed from the films during annealing to where ^{18}O was incorporated [Fig. 8(b)], it is possible to conclude that both processes occur more or less in the same regions of the Si_3N_4 films. This indicates that during the ^{18}O annealing, oxygen is incorporated in the same region where nitrogen is removed, in a solid-gas reaction, thus probably forming silicon oxynitride (between 1 and 8 nm thick) of variable composition near the Si_3N_4 surface. This great oxidation resistance and some possible solid-gas reactions between Si_3N_4 and O_2 has been reported[46] in β-Si_3N_4–$Y_2Si_2O_7$ ceramics annealed in air for different annealing times at 1000 and 1200 °C. Nevertheless, the gradual interface between the silicon oxynitride layer formed during annealing and the silicon nitride film should lead to a good adhesion between them. This should improve the solid lubricant effect of the silicon oxynitride layer in tribological applications at high temperatures, as reported for bulk Si_3N_4.[45]

To confirm the hypothesis of silicon oxynitride formation during annealing, XPS measurements were performed to evaluate the N and Si chemical ambient in the annealed and as-deposited films. Figure 10(a) shows the photoelectron region for Si 2*p* for a Si_3N_4 deposited at 200 °C for 120 s (solid circles, about 192 nm thick) and after $^{18}O_2$ annealing

[This article is copyrighted as indicated in the article. Reuse of AIP content is subject to the terms at: http://scitation.aip.org/termsconditions. Downloaded to] IP: 200.130.19.173 On: Fri, 21 Mar 2014 14:04:44

at 1000 °C (solid triangles). In the as-deposited sample we identify one single component attributed to Si bonded to N in the form of stoichiometric silicon nitride,[47,48] confirming our RBS results. After $^{18}O_2$ annealing at 1000 °C, a shift of this single component to higher binding energies is observed. This is a clear evidence of reaction between oxygen from the gas phase and the silicon nitride film, forming SiO_xN_y, which confirms our assumption. Figure 10(b) shows the photoelectron region for N 1*s* for the same sample, Si_3N_4 as-deposited (solid circles) and after $^{18}O_2$ annealing at 1000 °C (solid triangles). The as-deposited sample also presents a single N chemical state attributed to N bonded to Si in stoichiometric silicon nitride. When the sample is submitted to $^{18}O_2$ annealing at 1000 °C two conclusion can be made, (i) reduction of the N content near the film surface, since the photoelectron intensity of the annealed sample is lower than the as-deposited sample and (ii) shift of the single component to a higher binding energy, indicating the formation of silicon oxynitride.

VI. CONCLUSION

In summary, we investigated the physicochemical, structural, and mechanical properties of Si_3N_4 films before and after $^{18}O_2$ annealing. Films were stoichiometric for a substrate temperature range of 100–500 °C and essentially amorphous, except for the sample deposited at 500 °C, where some diffraction peaks from the α-Si_3N_4 phase are observed. Hardness and reduced elastic modulus variations with substrate temperature were also observed, which are attributed to changes in the internal stress of the films. A maximum hardness of 22 GPa was observed for the sample deposited at a substrate temperature of 200 °C, which leads to an elastic strain to failure of 0.25 GPa. After $^{18}O_2$ annealing at 1000 °C, the hardness of Si_3N_4 films deposited at different substrate temperature where seen to increase, converging to 21 GPa, which is a very interesting effect for high temperature applications, since most of the coatings suffer significant hardness reduction at this temperature. Moreover, oxygen is observed to incorporate only in 7.5 nm from the film surface, even after annealing for 1 h, indicating a high oxidation resistance of the Si_3N_4 coating. The hardness modulation after annealing was explained based on two competitive processes, the crystallization of the films, which led to an increase in hardness and to oxidation of the film and relaxation of the internal stress, leading to a decrease in hardness. These competitive processes keep the hardness figures close to 21 GPa for all investigated films after 1000 °C annealing, since at this temperature the crystallization of the film is favored. Finally, the H^3/E^2 figures almost doubles after the high temperature annealing which is one more desirable affect for high temperatures applications. The present results may also help to understand the superhardness of Si_3N_4/TiN multilayers, since it is important to know the properties of each individual layer in order to completely explain the still open issue of multilayer superhardness. Nevertheless, the promising mechanical properties of the Si_3N_4 as a coating for high temperature applications were demonstrated. Tribological characterization (nanowear and friction coefficient) of the films, before and after annealing, is in progress in our laboratory in order to demonstrate the full potentiality of Si_3N_4 as a hard coating for high temperature applications.

ACKNOWLEDGMENTS

The authors would like to acknowledge MCT/CNPq and CAPES for financial support.

[1] Y. C. Chim, X. Z. Ding, X. T. Zeng, and S. Zhang, Thin Solid Films **517**, 4845 (2009).
[2] S. Veprek and M. J. G. Veprek-Heijman, Surf. Coat. Technol. **202**, 5063 (2008).
[3] P. E. Hovsepian and W.-D. Münz, *Nanostructured Coatings* (Springer, New York, 2006).
[4] V. Derflinger, H. Brändle, and H. Zimmermann, Surf. Coat. Technol. **113**, 286 (1999).
[5] H. Hoche, D. Allebrandt, M. Bruns, R. Riedel, and C. Fasel, Surf. Coat. Technol. **202**, 5567 (2008).
[6] C. A. Powell and B. D. Morreale, MRS Bull. **33**, 309 (2008).
[7] M. B. da Silva and J. Wallbank, J. Mater. Process. Technol. **88**, 195 (1999).
[8] L. Yu, S. Dong, J. Xu, and I. Kojima, Thin Solid Films **516**, 1864 (2008).
[9] T. Polcar, R. Martinez, T. Vítü, L. Kopecký, R. Rodriguez, and A. Cavaleiro, Surf. Coat. Technol. **203**, 3254 (2009).
[10] A. Ziegle, J. C. Idrobo, M. K. Cinibulk, C. Kisielowski, N. D. Browning, and R. O. Ritchie, Science **306**, 1768 (2004).
[11] H. Schmidt, W. Gruber, G. Borchardt, M. Bruns, M. Rudolphi, and H. Baumann, Thin Solid Films **450**, 346 (2004).
[12] Y. Toivola, J. Thurn, and R. F. Cook, J. Appl. Phys. **94**, 6915 (2003).
[13] H. Chen, J. Liu, and W. Huang, Mater. Sci. Eng., A **415**, 291 (2006).
[14] Y. Liu, I.-K. Lin, and X. Zhang, Mater. Sci. Eng., A **489**, 294 (2008).
[15] P. Kroll, J. Non-Cryst. Solids **351**, 1127 (2005).
[16] V. Vila, D. Caceres, and C. Prieto, J. Appl. Phys. **94**, 7868 (2003).
[17] F. H. P. M. Habraken and A. E. T. Kuiper, Mater. Sci. Eng. R. **12**, 123 (1994).
[18] C. Savall, J. C. Bruyère, and J. P. Storquet, Thin Solid Films **260**, 174 (1995).
[19] A. Leyland and A. Matthews, Wear **246**, 1 (2000).
[20] F. Lv, S. P. Wen, R. L. Zong, F. Zeng, Y. Gao, and F. Pan, Surf. Coat. Technol. **202**, 3239 (2008).
[21] J. Suna, J. Musil, V. Ondok, and J. G. Han, Surf. Coat. Technol. **200**, 6293 (2006).
[22] Y. Pauleau and F. Thiery, Surf. Coat. Technol. **180–181**, 313 (2004).
[23] J. Soldán and J. Musil, Vacuum **81**, 531 (2006).
[24] S. Yang, Y. Chang, D. Lin, D. Wang, and W. Wu, Surf. Coat. Technol. **202**, 2176 (2008).
[25] L. C. Feldman, J. W. Mayer, and S. T. Picraux, *Materials Analysis by Ion Channeling* (Academic, New York, 1982).
[26] L. G. Parratt, Phys. Rev. **95**, 359 (1954).
[27] I. J. R. Baumvol, Surf. Sci. Rep. **36**, 1 (1999).
[28] R. P. Pezzi, P. L. Grande, and M. Copel, Surf. Sci. **601**, 5559 (2007).
[29] S. Hao, B. Delley, S. Veprek, and C. Stampfl, Phys. Rev. Lett. **97**, 086102 (2006).
[30] C. W. M. e Silva, E. Alves, A. R. Ramos, C. S. Sandu, and A. Cavaleiro, Vacuum **83**, 1213 (2009).
[31] W. J. Gunning, R. L. Hall, F. J. Woodberry, W. H. Southwell, and N. S. Gluck, Appl. Opt. **28**, 2945 (1989).
[32] P. Walsh, A. Omeltchenko, R. K. Kalia, A. Nakano, P. Vashista, and S. Saini, Appl. Phys. Lett. **82**, 118 (2003).
[33] P. Wei, L. Chen, A. Okubo, and T. Hirai, Mater. Lett. **49**, 239 (2001).
[34] H. Huang, K. J. Winchester, A. Suvorova, B. R. Lawn, Y. Liu, X. Z. Du, J. M. Dell, and L. Faraone, Mater. Sci. Eng., A **435–436**, 453 (2006).
[35] V. Verlaan, R. Bakker, C. H. M. van der Werf, Z. S. Houweling, Y. Mai, J. K. Rath, and R. E. I. Schropp, Surf. Coat. Technol. **201**, 9285 (2007).
[36] J. A. Taylor, J. Vac. Sci. Technol. A **9**, 2464 (1991).
[37] Y. G. Shen, Mater. Sci. Eng., A **359**, 158 (2003).
[38] G. L. Huffman, D. E. Fahnline, R. Messier, and L. J. Pilione, J. Vac. Sci. Technol. A **7**, 2252 (1989).
[39] Y. Okada and Y. Jukumaru, J. Appl. Phys. **56**, 314 (1984).
[40] R. M. Williams, J. Am. Ceram. Soc. **63**, 108 (1980).

[This article is copyrighted as indicated in the article. Reuse of AIP content is subject to the terms at: http://scitation.aip.org/termsconditions. Downloaded to] IP: 200.130.19.173 On: Fri, 21 Mar 2014 14:04:44

[41]P. J. Martin, A. Bendavid, and T. J. Kinder, Surf. Coat. Technol. **81**, 36 (1996).
[42]L. Karlsson, L. Hultman, and J.-E. Sundgren, Thin Solid Films **371**, 167 (2000).
[43]H.-M. Tung, J.-H. Huang, D.-G. Tsai, C.-F. Ai, and G.-P. Yu, Mater. Sci. Eng., A **500**, 104 (2009).
[44]M. Lattemann, S. Ulrich, H. Holleck, M. Stüber, and H. Lesite, Diamond Relat. Mater. **11**, 1248 (2002).
[45]A. Skopp, M. Woydt, and K.-H Habig, Wear **181/183**, 571 (1995).
[46]S. P. Taguchi and S. Ribeiro, J. Mater. Process. Technol. **147**, 336 (2004).
[47]J. Finster, E.-D. Klimkenberg, J. Heeg, and W. Braun, Vacuum **41**, 1586 (1990).
[48]D. S. Blair, J. W. Rogers, Jr., and C. H. F. Peden, J. Appl. Phys. **67**, 2066 (1990).

[This article is copyrighted as indicated in the article. Reuse of AIP content is subject to the terms at: http://scitation.aip.org/termsconditions. Downloaded to] IP: 200.130.19.173 On: Fri, 21 Mar 2014 14:04:44